ADVANCED FUNCTIONAL MATERIALS

Supporting Information

for *Adv. Funct. Mater.*, DOI: 10.1002/adfm.201707491

Transparent, Anisotropic Biofilm with Aligned Bacterial Cellulose Nanofibers

*Sha Wang, Tian Li, Chaoji Chen, Weiqing Kong, Shuze Zhu, Jiaqi Dai, Alfredo J. Diaz, Emily Hitz, Santiago D. Solares, Teng Li, and Liangbing Hu**

Supporting Information

Transparent, Anisotropic Biofilm with Aligned Bacterial Cellulose Nanofibers

Sha Wang[1(a)], Tian Li[1(a)], Chaoji Chen[1(a)], Weiqing Kong[1(a)], Shuze Zhu[2], Jiaqi Dai[1], Alfredo J. Diaz[3], Emily Hitz[1], Santiago D. Solares[3], Teng Li[2], Liangbing Hu*[,1]

[1]Department of Materials Science and Engineering, University of Maryland College Park, College Park, Maryland, 20742

[2]Department of Mechanical Engineering, University of Maryland College Park, College Park, Maryland, 20742

[3]Department of Mechanical and Aerospace Engineering, The George Washington University, Washington, District of Columbia, 20052

[(a)] These authors contributed equally to this work.

* Correspondence: binghu@umd.edu

BC pellicle fabrication.

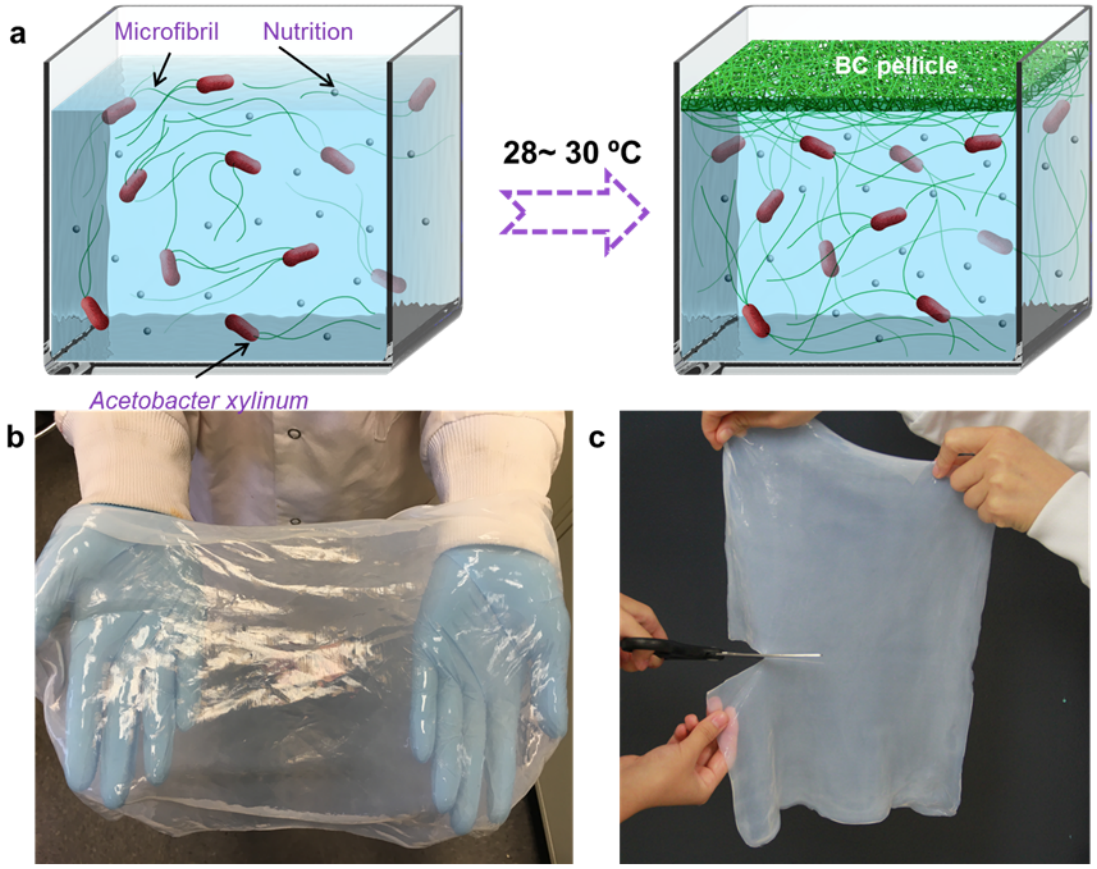

Figure S1. Through a fermentation process (a) a large piece of purified BC pellicle (b) with 99.4% of water content can be large-scale generated, which greatly reduces the cost for the production of transparent and ultra-strong film. BC transparent films are prepared by cutting a piece of purified BC pellicle into a rectangular shape of size 20 mm × 70 mm (c), then wet-drawn until the strain of the sample reached 20%, 30%, and 40%, respectively.

Stretching test setup

A schematic of the stretching process is shown in Figure S2 (a). The wet-drawing strain is defined as the percentage of length difference before and after drawing divided by the initial length of the BC pellicle. Figure S2 (b) shows a strip of BC pellicle (20 mm×70 mm) mounted between two grips. The bottom grip is fixed on the base and the top grip can be displaced up and down. After stretching, a wide BC strip becomes narrower and longer.

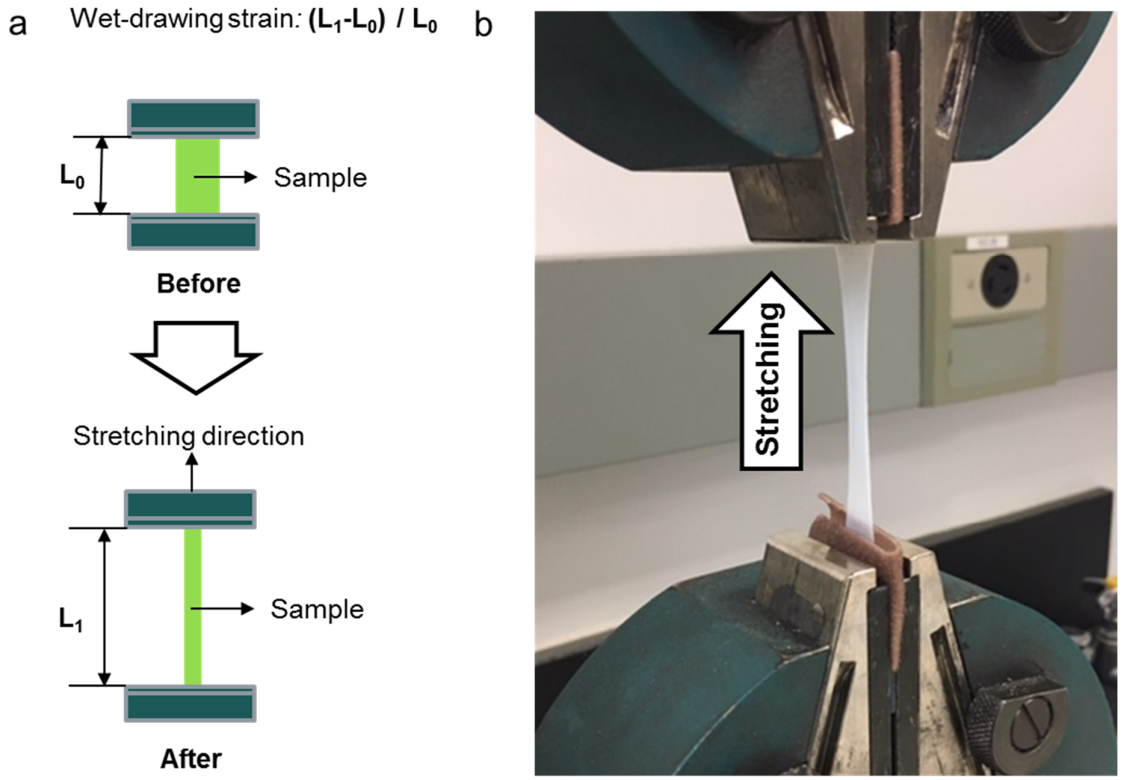

Figure S2. (a) Schematic of the stretching process and the definition of wet-drawing strain. (b) A BC pellicle is mounted between two grips, then becomes longer and narrower due to stretching caused by upward motion of the top grip.

Mechanical performance of wet BC pellilces

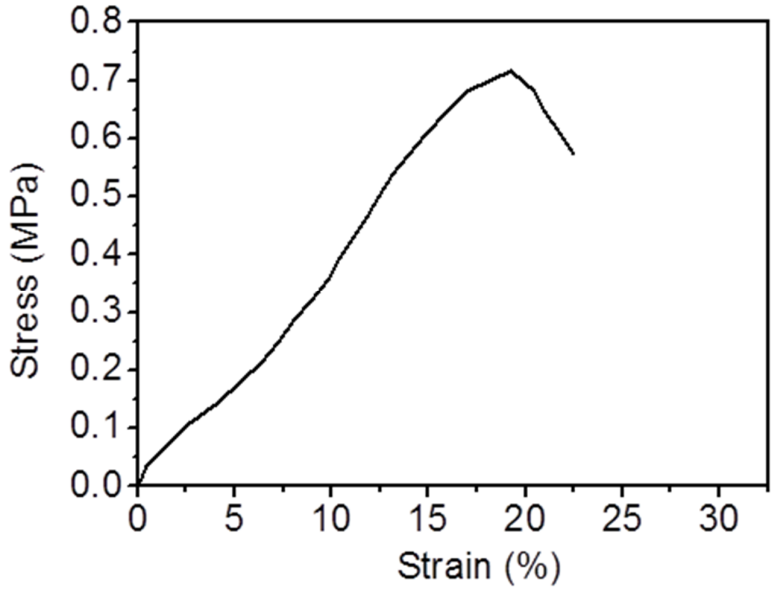

Figure S3. Stress-strain curve for wet BC pellicle. A BC pellicle with a width of 2 cm was stretched using a tensile test machine at a gauge length of 60 mm. A maximum wet-drawing strain of around 20% was observed before fracture of the cellulose nanofibrils.

SEM image of 40% stretched BC film at a low magnification.

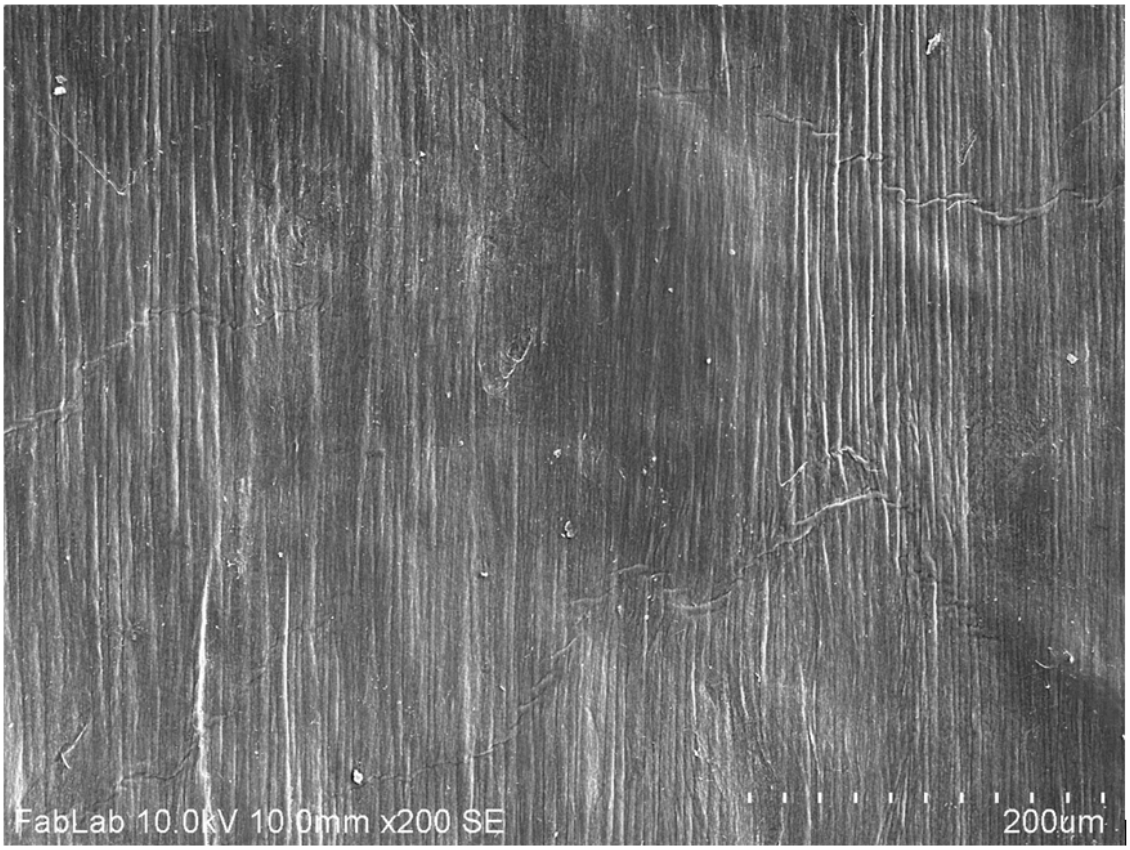

Figure S4. FE–SEM image of the surface of the 40% stretched BC film exhibiting an aligned pattern. The BC film is made from cutting and stretching the purified BC pellicle shown in Figure S1.

AFM images of BC films before and after alignment.

The surface morphologies of the resulting BC films under different wet-drawing strain levels are further analyzed by AFM (Figure S5). The as-grown BC film (0% in Figure S5) shows an isotropic structure, which is composed of randomly distributed nanofibrils. As for the 20% stretched sample, an increased degree of nanofibril orientation can be observed. Upon further increasing the drawing level, a well-aligned structure is clearly observed (30%, and 40% in Figure S5). As can be seen, the 40% stretched sample clearly shows a preferential orientation of the highly-aligned nanofibrils in the drawing direction.

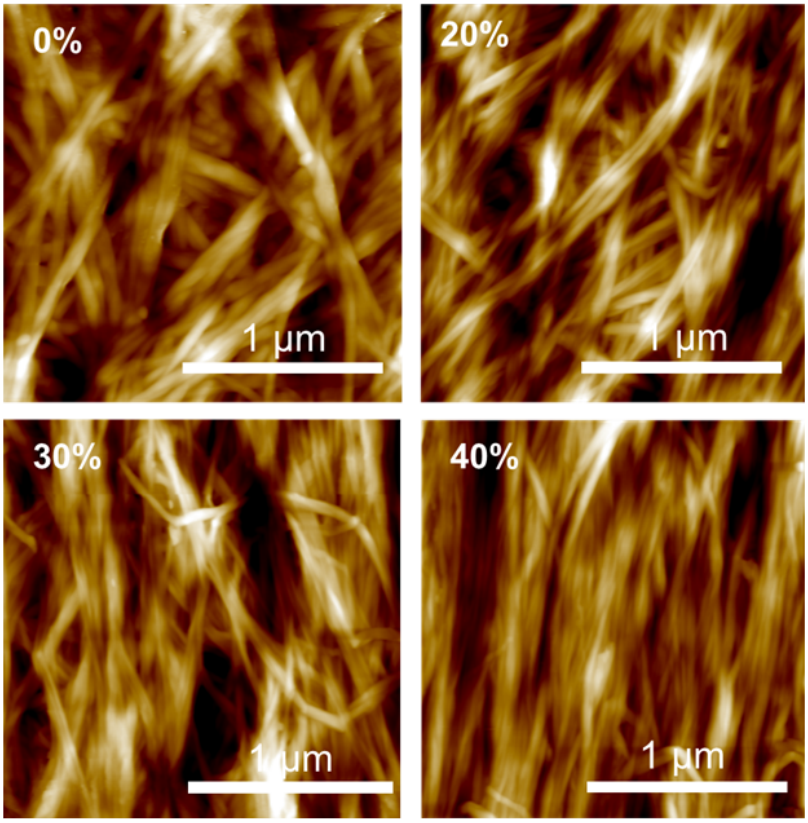

Figure S5. Typical AFM height images of BC films surfaces under 0%, 20%, 30%, and 40% wet-drawing strain, respectively, illustrating the increasing alignment with higher wet-drawing strain.

SAXS 2D patterns of BC films before and after alignment.

The original BC film shows a ring diffraction pattern, demonstrating a random structure. Upon increasing wet-drawing strain, the 2D diffraction patterns are deformed more and more, suggesting an alignment at the microscopic level, which is consistent with the previous SEM results.

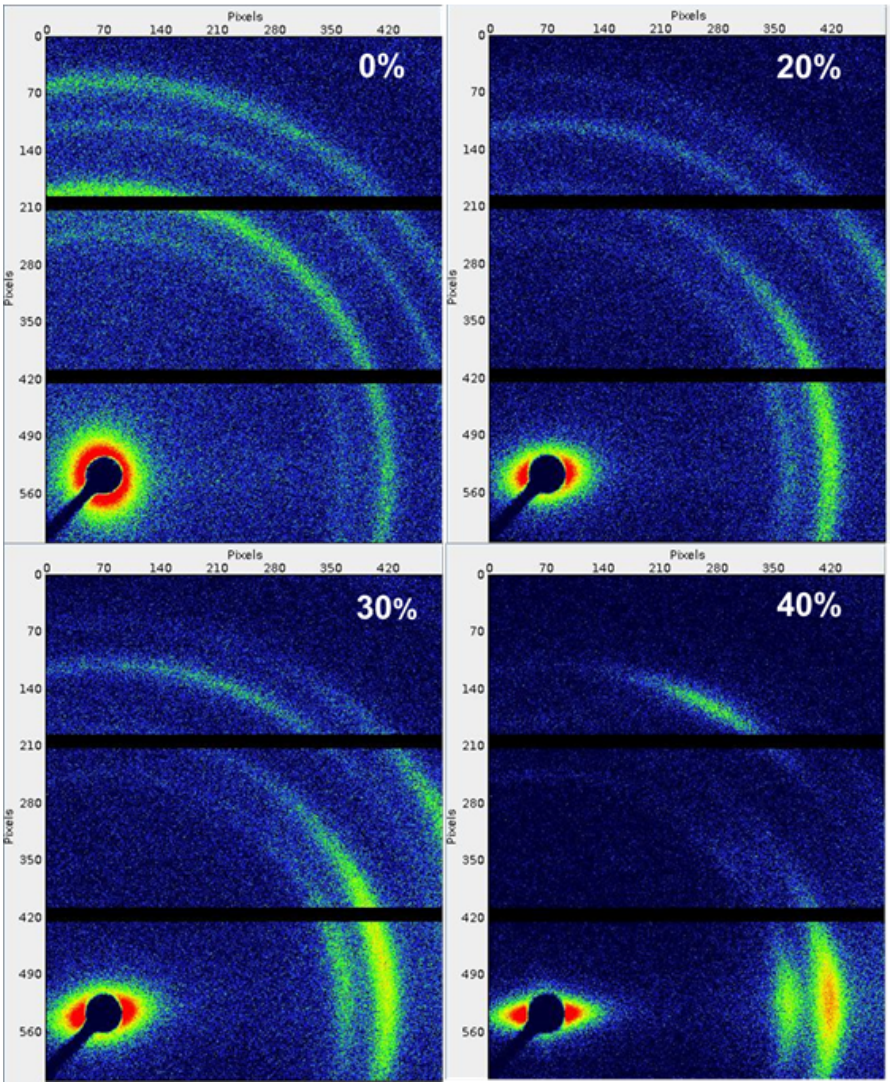

Figure S6. SAXS images of BC films before and after alignment. Typical SAXS patterns obtained for BC films under 0%, 20%, 30%, and 40% wet-drawing strain. The gradual deformation of 2D patterns (from 0% to 40%) indicates a clear trend of increasing alignment.

Fracture surface of aligned BC film

Figure S7 shows the morphology of BC fibers on the fracture surface of 40% wet-drawing BC film after stretching test. BC nanofibrils bundles are well parallel to each other due to the alignment process. The inset shows a photograph of the aligned BC film after a stretching test. The yellow box indicates the observation site under the optical microscope.

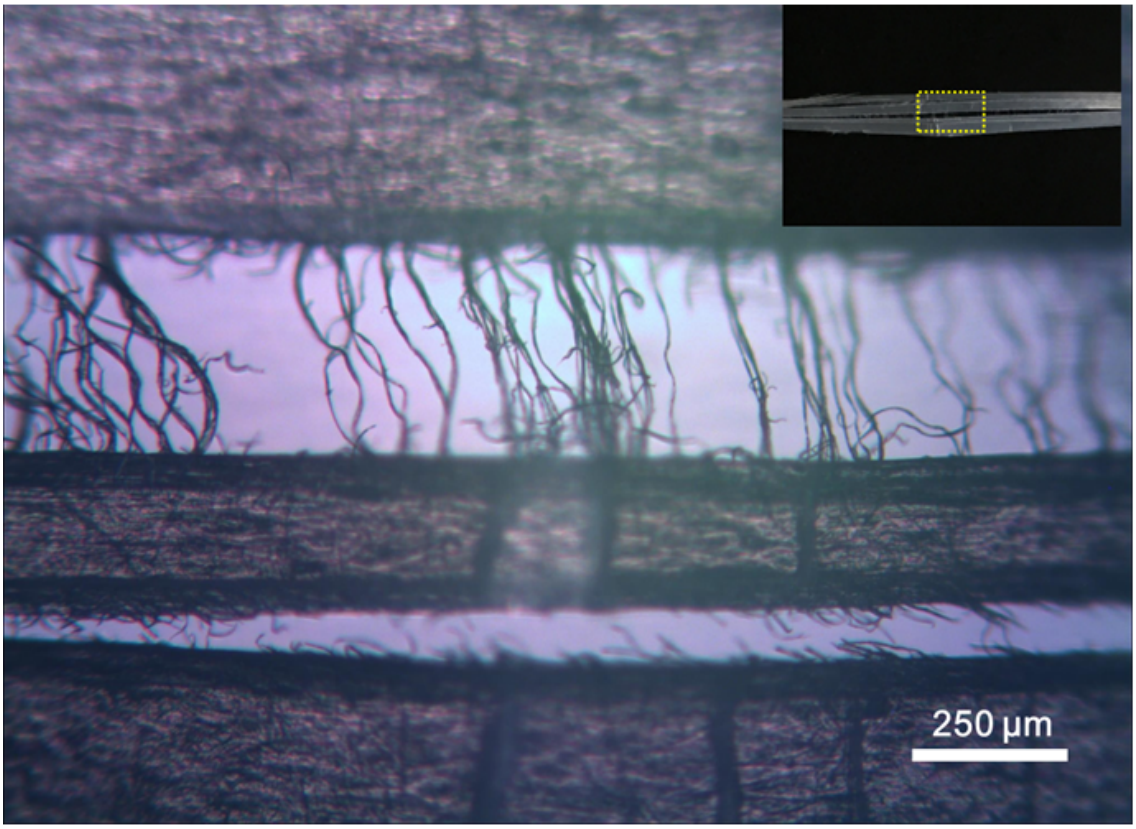

Figure S7. Morphology of fracture surface of aligned BC film at 40% wet-drawing strain. An optical microscope image of an aligned BC after a stretching test, clearly showing that the strongly aligned BC fibers are parallel to each other.

Table S1. Comprehensive comparisons of our developed BC film with some typical previously reported BC films and other cellulose films.

Sample Name	**Fabrication Method**	**Microstructure**	**Mechanical properties (strength, toughness)**		**Fundamental insight (yes or no)**	**Refs**
Highly aligned BC film	**Well-developed stretching (stretching-shaking)**	**Well-aligned, compact**	**~1GPa**	**24.7 MJ m^{-3}**	**Yes**	**This work**
Oriented nanofibrous BC film	Stretching	Partially aligned	179 MPa	0.009 MJ m^{-3}	No	Ref. 1
Stretched BC arrays	Guided BC growth and wet-stretching	Partially aligned	260 MPa	3.5 MJ m^{-3}	No	Ref. 2
PEG grafted CNF ribbon	Stretching	Aligned	576 MPa	10.9 MJ m^{-3}	No	Ref. 3
NFC film	Axially drawing	Aligned	474 MPa	4.9 MJ m^{-3}	No	Ref. 4
NFC nanopaper	Cold drawing	Poor alignment	428 MPa	6.56 MJ m^{-3}	No	Ref. 5

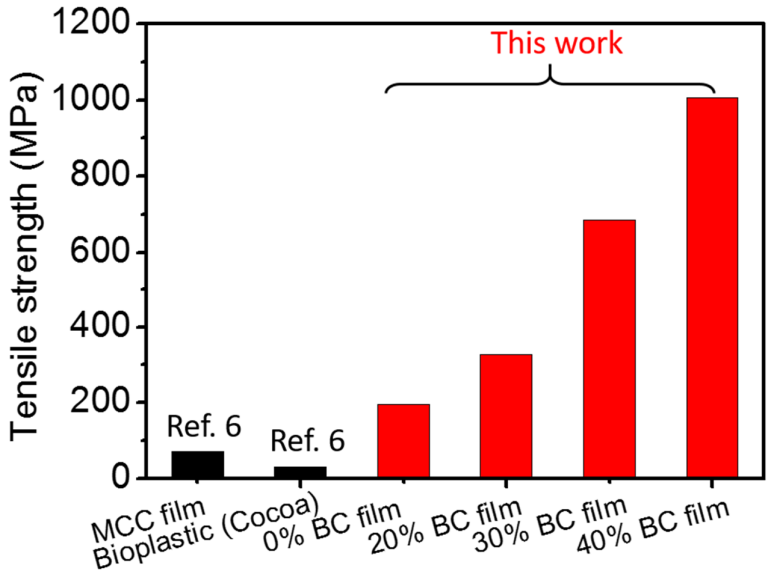

Figure S8. Mechanical properties comparison of BC films in our work with other cellulose films.

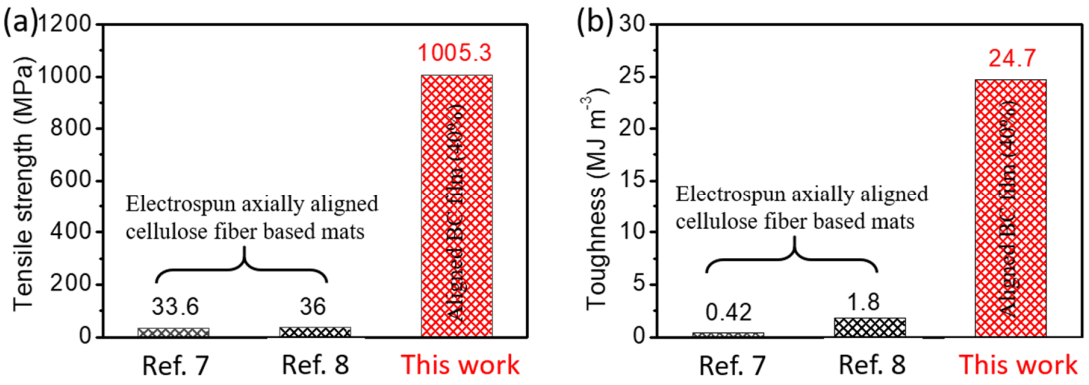

Figure S9. Mechanical properties comparison between the electrospun aligned cellulose nanofiber mats and our 40% BC film: (a) Tensile strength, (b) toughness.

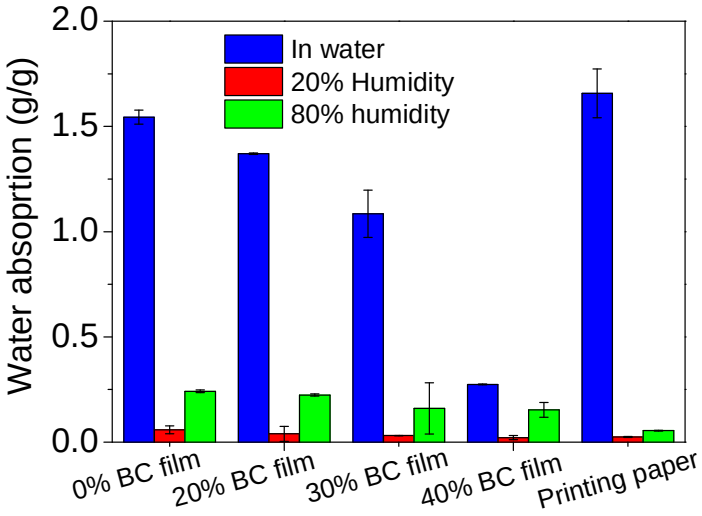

Figure S10. Water uptake of our BC films and the conventional printing paper under various humidity conditions.

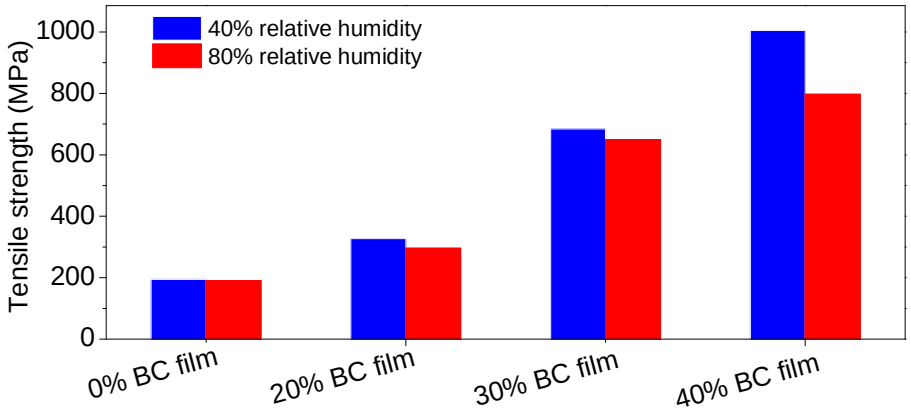

Figure S11. Humidity influence on the mechanical properties of our BC films.

Molecular dynamics simulation

The fully atomistic simulations used the ReaxFF potential[9] as implemented in the LAMMPS (Large-scale Atomic/Molecular Massively Parallel Simulator)[10] simulation package. The time step is 0.5 fs.

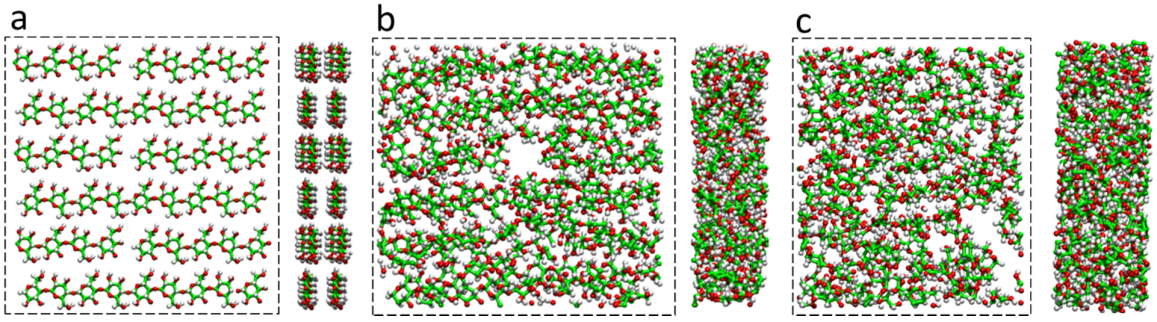

Figure S12. (a) Initial well-aligned model, for top view and side view. There are in total 12 cellulose chains (each has nine hexagonal rings) in a periodical simulation box (dashed line). Three alternating rows of cellulose chains are horizontally displaced about half the simulation box length. Green: carbon. Gray: hydrogen. Red: Oxygen. (b) Pressure-equilibrated well-aligned model. (c) Pressure-equilibrated random model.

The construction of the well-aligned model is shown in Figure S12 (a). For equilibration, the system is subjected to NPT-ensemble dynamics at a pressure of 1 atmosphere (normal pressure controlled independently) and at a temperature of 300K, using the Nosé-Hoover thermostat. The total duration of the run is 200,000 time steps. Figure S12 (b) shows the pressure-equilibrated structure. Then the mechanical deformation is applied by uniformly deforming the simulation box at a constant engineering strain rate of 0.0000025/fs, while the system is subjected to NVT ensemble with the temperature unchanged.

The construction of the randomly-dispersed model follows two steps: 1) construction of a very large simulation box and placement of 12 cellulose chains inside it so that initially they do not interact with each other. 2) execution of NVT simulation for a sufficiently long time for each cellulose chain to adopt its typical morphology. 3) execution of NVT simulations with gradual shrinking of the simulation box size so that the

cellulose chains start to aggregate. The target simulation box size is set to the one shown in Figure S12 (c). 4) Execution of NPT simulations to equilibrate the system. After this step, the mechanical deformation is applied in the same way as for the well-aligned model.

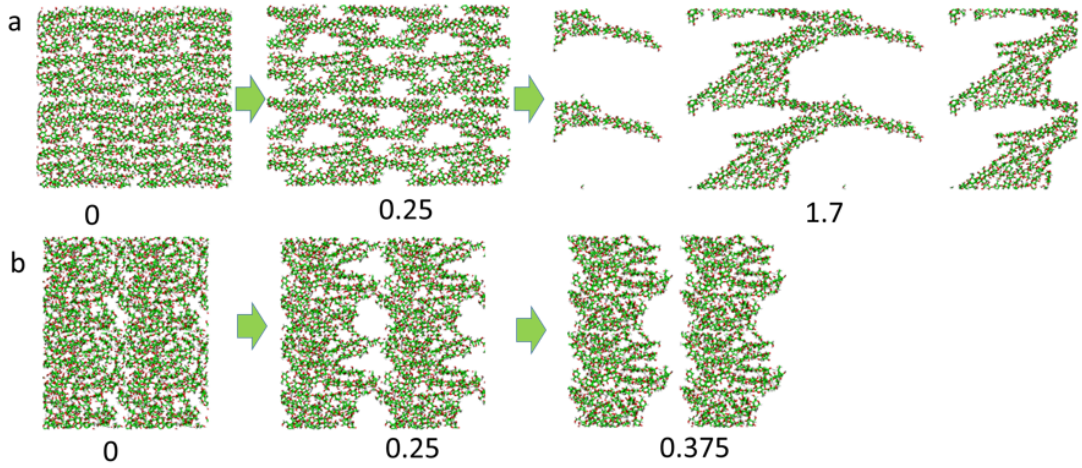

Figure S13. Deformation trajectory snapshots at different strains for the well-aligned (a), and random (b) models.

The deformation trajectory snapshots for the aligned and random models under consideration are shown in Figure S13. The virial stress is commonly used to relate to the macroscopic (continuum) stress to molecular dynamics computations.[11] At every time step during the loading, the virial stress per atom (with the units of pressure × atomic volume) is computed by the LAMMPS code. To reduce random and temperature-related stress fluctuations, we average the computed stress data every 30,000 time steps, by summing up the virial stress of every atom in the system and averaging over the occupied volume of all the atoms, which we take as the volume of the simulation box after equilibration. The loading is applied along the *x* direction and we plot the normal virial stress tensor component along the *x* direction against the engineering strain. The engineering strain is defined as the increment of the box size along the *x* direction divided by its initial length.

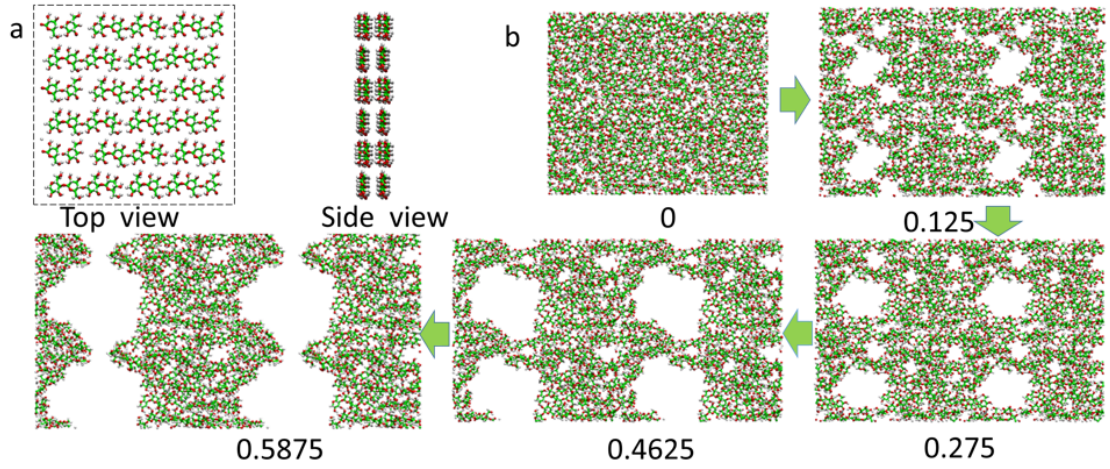

Figure S14. (a) A aligned-short model with four or five hexagonal rings (the cellulose chain is shorter than for the model shown in Figure S12 (a)). Top view and side view. (b) Deformation trajectory snapshots at different strains.

The top and side view of the aligned-short model with four or five hexagon rings is shown in Figure S14 (a). As observed from the deformation trajectory snapshots in Figure S14 (b), at a strain of 0.125, non-uniform deformation is already evident. For the model in Figure S13 (a), the deformation remains rather uniform even at a strain of 0.25. Such a difference in deformation mode causes a decrease in both maximum stress and toughness.

Light scattering setup

Figure S15 shows the light scattering setup, in which a 532 nm single mode laser (Thorlabs Inc.) was first collimated with a spot size around 200 μm before perpendicularly illuminating the samples. The incoming light rapidly diverges due to scattering within the samples.

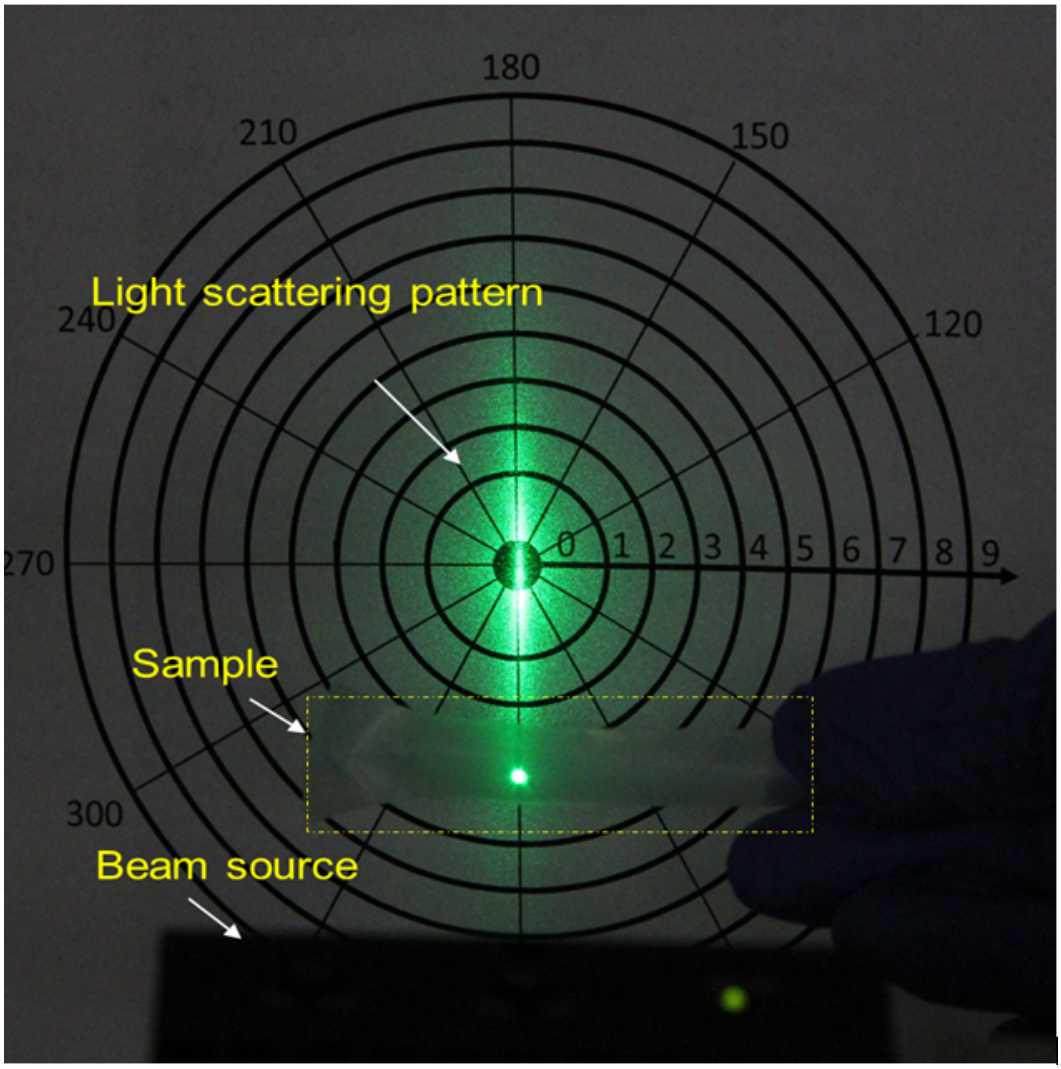

Figure S15. Light scattering setup. A green laser beam with a wavelength of 532 nm transmits through the stretched BC film and shows strong light scattering on a white screen. A 40% wet-stretched BC film is placed between a green laser beam source and a screen. Strong light scattering is observed. The yellow dashed line enclosing the sample is drawn as a visual guide.

Light scattering effects

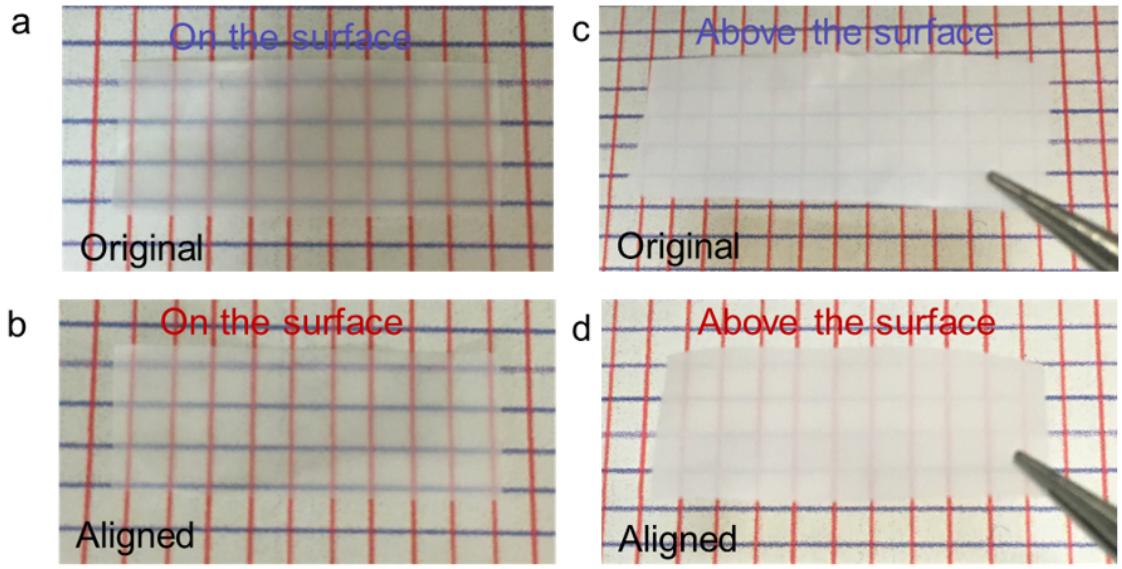

Figure S16. The original BC film is placed on (a) and above the surface (1 cm above) (b) of grids made up of parallel vertical red lines and parallel horizontal blue lines, respectively. The aligned BC film is placed on (c) and above the grid's surface (d). All lines can be clearly seen for both films when directly placing them on the surfaces of grids. For the aligned BC film, the vertical red lines are more visible than the horizontal blue lines due to anisotropic light scattering.

Figure S16 shows a unique scattering effect of the aligned BC film. Grids are made up of vertical red lines and horizontal blue lines. All lines can be clearly seen for both the original and aligned BC films when placing them directly on the surface of the grid lines (Figure S16 a, b). However, all grids lines become hazy when the original BC film is placed 1 cm above the surface due to the high transmittance haze (Figure S16 c, d). For the aligned BC film, the vertical red lines are much clearer while the horizontal blue lines appear more blurry due to anisotropic scattering effects, which are in accordance with the anisotropic haze effect shown in Figure 5a, d.

Supplementary References

[1] A. Nagashima, T. Tsuji, T. Kondo, *Carbohydr. Polym.* **2016**, *135*, 215.

[2] M. M. Rahman, A. N. Netravali, *ACS Macro. Lett.* **2016**, *5*, 1070.

[3] H. Tang, N. Butchosa, Q. Zhou, *Adv. Mater.* **2015**, *27*, 2070.

[4] C. Baez, J. Considine, R. Rowlands, *Cellulose* **2014**, *21*, 347.

[5] H. Sehaqui, N. Ezekiel Mushi, S. Morimune, M. Salajkova, T. Nishino, L. A. Berglund, *ACS Appl. Mater. Interfaces* **2012**, *4*, 1043.

[6] I. S. Bayer, S. Guzman-Puyol, J. A. Heredia-Guerrero, L. Ceseracciu, F. Pignatelli, R. Ruffilli, R. Cingolani, A. Athanassiou, *Macromolecules* **2014**, 47, 5135.

[7] X. He, Q. Xiao, C. Lu, Y. Wang, X. Zhang, J. Zhao, W. Zhang, X. Zhang, Y. Deng, *Biomacromolecules* **2014**, 15, 618.

[8] H. Q. Liao, Y. Q. Wu, M. Y. Wu, X. R. Zhan, H. Q. Liu, *Cellulose* **2012**, 19, 111.

[9] T. R. Mattsson, J. M. D. Lane, K. R. Cochrane, M. P. Desjarlais, A. P. Thompson, F. Pierce, G. S. Grest, *Phys. Rev. B* **2010**, 81, 054103.

[10] S. Plimpton, *J. Comput. Phys.* **1995**, 117, 1.

[11] D. Tsai, *J. Chem. Phys.* **1979**, 70, 1375.